Absorptive part of meson–baryon scattering amplitude and baryon polarization in chiral perturbation theory

Antonio O. Bouzas *
Departamento de Física Aplicada, CINVESTAV-IPN
Carretera Antigua a Progreso Km. 6, Apdo. Postal 73 "Cordemex"
Mérida 97310, Yucatán, México

Abstract

We compute the spin asymmetry and polarization of the final-state baryon in its rest frame in two-body meson–baryon low-energy scattering with unpolarized initial state, to lowest non-trivial order in BChPT. The required absorptive amplitudes are obtained analytically at one-loop level. We discuss the polarization results numerically for several meson–baryon processes. Even at low energies above threshold, where BChPT can reasonably be expected to be applicable, sizable values of polarization are found for some processes.

1 Introduction

Low-energy hadron dynamics is succesfully described by Chiral Perturbation Theory (ChPT), the effective field theory of meson strong, electromagnetic and weak interactions (see, *e.g.,* [1, 2, 3] for recent reviews, [4, 5] for textbook expositions). The effective chiral framework can also be extended to the one-baryon sector, where a fully relativistic Baryon Chiral Perturbation Theory (BChPT) has been formulated, describing baryon interactions at low energies (recent reviews are given in [6, 3]. The equivalent heavy-baryon approach is reviewed, *e.g.,* in [7]). As in virtually all areas of hadronic physics [8], in the low-energy regime spin phenomena are of great interest as probes of the structure and dynamics of baryons. Chiral effective theories are essential tools in the study of those phenomena and have been applied, for instance, to compute nucleon spin structure functions and spin-dependent polarizabilities [6].

From the experimental point of view, spin observables at low- and medium-energies have bee the subject of intensive studies in some cases, but data is scarce in others. There exists, for instance, a substantial body of data on analyzing powers in nucleon–pion scattering at energies around the Δ resonance peak (see [9, 10, 11] and refs. therein), and at lower energies [12, 13]. In the strange sector data on spin observables at low energies are definitely rare, though some exist [14].

In this paper we consider a particular aspect of hadron spin dynamics, the production of polarized baryons in unpolarized meson–baryon scattering, in BChPT. Such polarization effects are known to be large in the high energy regime [8, 15] where, unlike at low energy, the degrees of freedom relevant to the dynamics are the partonic ones. Here, we compute the spin asymmetry and polarization of the final-state baryon in its rest frame in low-energy two-body meson–baryon scattering with unpolarized initial state, to lowest non-trivial order in BChPT. Our main result is the expression for the spin asymmetry to that order in closed analytical form. From a more qualitative point of view, our main motivation is to ascertain what spin asymmetries and polarizations are obtained in BChPT, what physical mechanisms are responsible for them, how they depend on the kinematics of the scattering process (energy, scattering angle, and flavor), and what is the order of magnitude of the polarization effects obtained.

The paper is organized as follows. In the following section we present our notation and conventions, including our choice of flavor basis, the parameterization for the scattering amplitude and the related expressions for the spin asymmetry and polarization, and the tree-level amplitudes. The absorptive part of

*E-mail: abouzas@mda.cinvestav.mx

the amplitude is obtained analytically at one-loop level in Sect. 3. This result completes the calculation of the asymmetry and polarization at lowest non-trivial order in BChPT. In Sect. 4 we discuss our results in a more concrete setting, illustrating them with numerical computations of the polarization for several meson–baryon processes. In Sect. 5 we give some final remarks.

2 Scattering amplitude and polarization

The ground-state meson and baryon octets are described by standard [5] traceless 3×3 complex matrix fields ϕ and B, resp., with ϕ hermitian. We use the physical flavor basis

$$\begin{gathered} \beta^1 = \frac{1}{\sqrt{2}}\left(\lambda^1 + i\lambda^2\right), \quad \beta^1 = \beta^{2\dagger}\ , \quad \beta^3 = \lambda^3\ , \\ \beta^4 = \frac{1}{\sqrt{2}}\left(\lambda^4 + i\lambda^5\right), \quad \beta^5 = \beta^{4\dagger}\ , \quad \beta^6 = \frac{1}{\sqrt{2}}\left(\lambda^6 + i\lambda^7\right), \quad \beta^7 = \beta^{6\dagger}\ , \quad \beta^8 = \lambda^8\ , \end{gathered} \tag{1}$$

where λ^a are SU(3) Gell-Mann matrices. The real matrices β^a are not hermitian. Their hermitian conjugates form a basis that differs from $\{\beta^a\}_{a=1}^8$ only in its ordering. To distinguish field components with respect to each of those bases we use lower flavor indices for ${\beta^\dagger}_a$. Thus, meson and baryon fields are decomposed as[1] $\phi = \sum_b \phi_b \beta^b/\sqrt{2} = \sum_b \phi^b {\beta^\dagger}_b/\sqrt{2}$ and $B = \sum_a B_a \beta^a/\sqrt{2} = \sum_a B^a {\beta^\dagger}_a/\sqrt{2}$, with $\phi_b = \mathrm{Tr}\left({\beta^\dagger}_b \phi\right)/\sqrt{2}$, $\phi^b = \mathrm{Tr}\left(\beta^b \phi\right)/\sqrt{2}$, and similarly B_a and B^a. Baryon and meson states are denoted $|B^a(p,\sigma)\rangle$ and $|M^b(q)\rangle$, resp., with $\sigma = \pm 1/2$ the spin along a fixed spatial direction in the fermion rest frame, and p, q four-momenta. We always use hadron kets with an upper index, and bras with a lower one, with masses m_a and $\widetilde{m}_b$ for baryons and mesons resp. Free fields couple to one-particle states as $\langle 0|B_a(x)|B^c(p,\sigma)\rangle = \delta_a^c u(p,\sigma)\exp(-ipx)$ and $\langle 0|\phi_b(x)|M^c(q)\rangle = \delta_b^c \exp(-iqx)$.

Indices can be raised or lowered by means of the symmetric matrices $e^{ab} = \mathrm{Tr}\left(\beta^a\beta^b\right)/2 = \mathrm{Tr}\left({\beta^\dagger}_a{\beta^\dagger}_b\right)/2 = e_{ab}$ and $e_b^a = \delta_b^a$. In this basis the structure constants and the anticommutator constants in the fundamental representation are

$$\begin{aligned} [\beta^a,\beta^b] &= 2\sum_c {f^{ab}}_c \beta^c\ , & {f^{ab}}_c &= \frac{1}{4}\mathrm{Tr}\left({\beta^\dagger}_c[\beta^a,\beta^b]\right), \\ \{\beta^a,\beta^b\} &= 2\sum_c {d^{ab}}_c \beta^c + \frac{4}{3}e^{ab}\ , & {d^{ab}}_c &= \frac{1}{4}\mathrm{Tr}\left({\beta^\dagger}_c\{\beta^a,\beta^b\}\right). \end{aligned} \tag{2}$$

Similar definitions hold for ${f_a}^b{}_c$, ${d^a}_{bc}$, etc. The constants f^{abc} and d^{abc} (as well as $f_{abc} = -f^{abc}$ and $d_{abc} = d^{abc}$) are totally antisymmetric and symmetric, resp. Their numerical values are different from their Gell-Mann–basis analogs.

With the T-matrix defined in terms of the S-matrix as $S = I + i(2\pi)^4\delta(P_f - P_i)T$, the scattering amplitudes are given by T-matrix elements ${\mathcal{T}^{ab}}_{a'b'}(s,u;\sigma,\sigma') \equiv \langle B_{a'}(p',\sigma')M_{b'}(q')|T|B^a(p,\sigma)M^b(q)\rangle$ as functions of the Mandelstam invariants $s = (p+q)^2$, $u = (p-q')^2$ and the spin variables. The most general form for the two-body meson-baryon scattering amplitude consistent with Lorentz invariance and the discrete symmetries of the strong interactions is

$$\mathcal{T}^{ab}{}_{a'b'} = \overline{u}'(p',\sigma')\Gamma^{ab}{}_{a'b'}\,u(p,\sigma), \qquad \Gamma^{ab}{}_{a'b'} = {\Gamma_0}^{ab}{}_{a'b'} + {\Gamma_1}^{ab}{}_{a'b'}\not{p}_T\ , \tag{3a}$$

with p_T the total momentum, and $\Gamma^{ab}{}_{a'b'}$ depending only on s, u. Below we will make repeated use of the unitarity relation for two-body scattering amplitudes, involving an integration volume element depending on p_T, which justifies our choice of a parameterization of $\Gamma^{ab}{}_{a'b'}$ in terms of $\not{p}_T$. Complex conjugation of the first equality in (3a) yields the matrix element ${\mathcal{T}^\dagger}^{a'b'}{}_{ab} = \langle B_a(p,\sigma)M_b(q)|T^\dagger|B^{a'}(p',\sigma')M^{b'}(q')\rangle$ written as,

$${\mathcal{T}^\dagger}^{a'b'}{}_{ab} = \overline{u}(p,\sigma)\overline{\Gamma}^{a'b'}{}_{ab}\,u'(p',\sigma'), \qquad \overline{\Gamma}^{a'b'}{}_{ab} = \overline{\Gamma}_0{}^{a'b'}{}_{ab} + \overline{\Gamma}_1{}^{a'b'}{}_{ab}\not{p}_T = ({\Gamma_0}^{ab}{}_{a'b'})^* + ({\Gamma_1}^{ab}{}_{a'b'})^*\not{p}_T\ . \tag{3b}$$

[1] We do not use summation convention for flavor indices.

The dispersive and absorptive parts of the amplitude are then $\Gamma^{ab}{}_{a'b'} = \Gamma_D{}^{ab}{}_{a'b'} + i\Gamma_A{}^{ab}{}_{a'b'}$ with,

$$\begin{aligned}\Gamma_D{}^{ab}{}_{a'b'} &= \frac{1}{2}\left(\Gamma^{ab}{}_{a'b'} + \overline{\Gamma}^{a'b'}{}_{ab}\right) \doteq \mathrm{Re}\left(\Gamma_0{}^{ab}{}_{a'b'}\right) + \mathrm{Re}\left(\Gamma_1{}^{ab}{}_{a'b'}\right) \not{p}_T \ , \\ \Gamma_A{}^{ab}{}_{a'b'} &= \frac{1}{2i}\left(\Gamma^{ab}{}_{a'b'} - \overline{\Gamma}^{a'b'}{}_{ab}\right) \doteq \mathrm{Im}\left(\Gamma_0{}^{ab}{}_{a'b'}\right) + \mathrm{Im}\left(\Gamma_1{}^{ab}{}_{a'b'}\right) \not{p}_T \ .\end{aligned} \tag{4}$$

In this equation, and in what follows, the symbol "$\doteq$" means that equality holds when both sides are sandwiched between $\overline{u}'(p',\sigma')$ and $u(p,\sigma)$. Although time-reversal invariance is already taken into account in the Dirac structure of (3), it also implies restrictions on the flavor dependence of the amplitude. In the flavor basis (1), time-reversal invariance is expressed as

$$\overline{u}'(p',\sigma')\left(\Gamma_0{}^{ab}{}_{a'b'} + \Gamma_1{}^{ab}{}_{a'b'}\not{p}_T\right)u(p,\sigma) = \overline{u}'(p',\sigma')\left(\Gamma_0{}^{a'b'}{}_{ab} + \Gamma_1{}^{a'b'}{}_{ab}\not{p}_T\right)u(p,\sigma), \tag{5}$$

where we again omitted the arguments s, u, which are invariant under time inversion.

The Dirac spinor $u'(p',\sigma')$ satisfies the polarization equation $\gamma_5 \not{s}' u'(p',\sigma') = -2\sigma' u'(p',\sigma')$, where s'^μ is the spin four-vector defined by the condition that in the fermion rest frame $s'^\mu = (0,\hat{s}'_*)$ with $\hat{s}'_*$ the versor lying on the fixed spin-quantization axis. The following relations then hold, $s'^\mu s'_\mu = -1$, $s'^\mu p'_\mu = 0$, and

$$u'(p',\sigma')\overline{u}'(p',\sigma') = \frac{1}{2}(\not{p}' + m_{a'})(1 - 2\sigma'\gamma_5\not{s}'). \tag{6}$$

The total unpolarized squared amplitude, symbolically denoted $|\mathcal{T}|^2$, is given by

$$\begin{aligned}|\mathcal{T}|^2 &\equiv \frac{1}{2}\sum_{\sigma,\sigma'}\mathcal{T}^{ab}{}_{a'b'}\mathcal{T}^{\dagger a'b'}{}_{ab} = \frac{1}{2}\mathrm{Tr}\left(\Gamma^{ab}{}_{a'b'}(\not{p}+m_a)\overline{\Gamma}^{a'b'}{}_{ab}(\not{p}'+m_{a'})\right) \\ &= C_{00}\left|\Gamma_0{}^{ab}{}_{a'b'}\right|^2 + C_{11}\left|\Gamma_1{}^{ab}{}_{a'b'}\right|^2 + 2C_{01}\mathrm{Re}\left(\Gamma_0{}^{ab}{}_{a'b'}\Gamma_1{}^{ab}{}_{a'b'}{}^*\right),\end{aligned} \tag{7a}$$

with

$$\begin{gathered}C_{00} = ((m_a+m_{a'})^2 - t), \qquad C_{01} = m_a(s + m_{a'}^2 - \widetilde{m}_{b'}^2) + m_{a'}(s + m_a^2 - \widetilde{m}_b^2), \\ C_{11} = (s + m_{a'}^2 - \widetilde{m}_{b'}^2)(s + m_a^2 - \widetilde{m}_b^2) + s\left(t - (m_{a'} - m_a)^2\right).\end{gathered} \tag{7b}$$

From (3) and (6) the spin asymmetry $\mathcal{A}$ for unpolarized two-body scattering is written as,

$$\begin{aligned}\mathcal{A} &\equiv \frac{1}{2}\sum_{\sigma,\sigma'}(2\sigma')\mathcal{T}^{ab}{}_{a'b'}\mathcal{T}^{\dagger a'b'}{}_{ab} = \frac{1}{2}\mathrm{Tr}\left(\Gamma^{ab}{}_{a'b'}(\not{p}+m_a)\overline{\Gamma}^{a'b'}{}_{ab}(\not{p}'+m_{a'})\ \not{s}'\gamma_5\right) \\ &= -i\left(\mathrm{Re}\left(\Gamma_0{}^{ab}{}_{a'b'}\right)\mathrm{Im}\left(\Gamma_1{}^{ab}{}_{a'b'}\right) - \mathrm{Im}\left(\Gamma_0{}^{ab}{}_{a'b'}\right)\mathrm{Re}\left(\Gamma_1{}^{ab}{}_{a'b'}\right)\right)\mathrm{Tr}\left(\not{p}\not{p}_T\not{p}'\ \not{s}'\gamma_5\right).\end{aligned} \tag{8}$$

Since

$$\begin{aligned}-i\mathrm{Tr}\left(\not{p}\not{p}_T\not{p}'\ \not{s}'\gamma_5\right) &= 4\varepsilon^{\alpha\beta\gamma\delta}p_\alpha p_{T\beta}p'_\gamma s'_\delta \\ &= 4m_{a'}\sqrt{\vec{p}^{\,2}\vec{q}^{\,2} - (\vec{p}\cdot\vec{q})^2}\ \hat{s}'_*\cdot\hat{n}\ , \qquad \hat{n} = \frac{\vec{q}\wedge\vec{p}}{|\vec{q}\wedge\vec{p}|}\ , \qquad (\mathrm{lab}')\end{aligned} \tag{9}$$

where the second equality holds in the rest frame of the final baryon (henceforth "lab′" frame), we see that for an unpolarized initial state the final-state spin asymmetry in the lab′ frame lies along the direction $\hat{n}$ orthogonal to the plane of the reaction. We denote $\mathcal{A}'_*$ the asymmetry $\mathcal{A}$ expressed in lab′ frame, as in (9), and with $\hat{s}'_* = \hat{n}$. The polarization of the final baryon along the direction $\hat{n}$ in its rest frame is then

$$\mathcal{P}'_* = \frac{\mathcal{A}'_*}{|\mathcal{T}|^2}\ . \tag{10}$$

We see from the second line of (8) that $\mathcal{A}'_*$ and $\mathcal{P}'_*$ vanish unless real particles are created in intermediate states. Indeed, if only virtual–particle intermediate states are possible then the imaginary parts $\mathrm{Im}(\Gamma_{0,1}) = 0$ in (8), leading to a vanishing asymmetry. This occurs, in particular, at tree level. To obtain $\mathcal{A}'_*$ and $\mathcal{P}'_*$ to lowest non-trivial order we must compute the dispersive part of the amplitude at tree level, and its absorptive part at one loop.

2.1 Tree-level amplitudes

The Lagrangian of fully relativistic Baryon Chiral Perturbation Theory (BChPT) is written as a sum $\mathcal{L} = \mathcal{L}_M + \mathcal{L}_{MB}$ of a purely mesonic Lagrangian $\mathcal{L}_M$ and a meson–baryon one $\mathcal{L}_{MB}$. The mesonic Lagrangian to $\mathcal{O}(q^4)$[2] was first obtained in [17, 18]. The meson–baryon Lagrangian $\mathcal{L}_{MB}$ has been given to $\mathcal{O}(q^3)$ in the three-flavor case in [19, 20, 21] (and in [16] for two flavors). Here we discuss the tree-level amplitudes for meson–baryon scattering obtained from $\mathcal{L}$.

In the parameterization (3a) it is convenient to write $\mathcal{T}^{ab}{}_{a'b'}$ as a sum over Feynman graphs $\mathcal{G}$, explicitly factoring the flavor coefficients from interaction vertices,

$$\Gamma^{ab}{}_{a'b'} \doteq \Gamma_0{}^{ab}{}_{a'b'} + \Gamma_1{}^{ab}{}_{a'b'} \not{p}_T = \sum_{\mathcal{G}} \sum_{\{I\}_{\mathcal{G}}} \mathcal{F}_{(\mathcal{G})}{}^{ab}{}_{a'b'}{}^{\{I\}} \left(\widehat{\Gamma}^{\{I\}}_{(\mathcal{G})0} + \widehat{\Gamma}^{\{I\}}_{(\mathcal{G})1} \not{p}_T \right). \tag{11}$$

The index $\mathcal{G}$ in (11) runs over all Feynman graphs contributing to the amplitude $\mathcal{T}^{ab}{}_{a'b'}$. The second sum runs over a set $\{I\}_{\mathcal{G}}$ of internal flavor indices for each diagram $\mathcal{G}$. In the flavor limit the reduced form factors $\widehat{\Gamma}^{\{I\}}_{(\mathcal{G})0,1}$ carry only internal flavor indices but, in fact, they also depend on a, a' through their dependence on initial and final baryon masses. At tree level $\mathcal{G}$ takes the values c (contact-interaction diagram), s and u. The set $\{I\}_c$ is empty, and each of $\{I\}_{s,u}$ contains only one flavor index originating in the mass of the internal baryon line.[3] The tree-level amplitude $\mathcal{T}^{ab}{}_{a'b'}$ can then be written as,

$$\mathcal{F}_{(c)}{}^{ab}{}_{a'b'} = \sum_d f_{b'}{}^{b}{}_{d} f^{da}{}_{a'} \ , \quad \widehat{\Gamma}_{(c)0} = -\frac{1}{2f^2}(m_a + m_{a'}) \ , \quad \widehat{\Gamma}_{(c)1} = \frac{1}{f^2} \ , \tag{12a}$$

$$\mathcal{F}_{(s)}{}^{ab}{}_{a'b'}{}^{\{d\}} = \left(Dd^{ba}{}_{d} + Ff^{ba}{}_{d} \right) \left(Dd^{d}{}_{b'a'} - Ff^{d}{}_{b'a'} \right), \quad \widehat{\Gamma}^{\{d\}}_{(s)1} = -\frac{1}{f^2} \left(1 + \frac{(m_{a'} + m_d)(m_a + m_d)}{s - m_d^2} \right),$$
$$\widehat{\Gamma}^{\{d\}}_{(s)0} = \frac{1}{f^2} \left(m_a + m_{a'} + m_d + m_d \frac{(m_{a'} + m_d)(m_a + m_d)}{s - m_d^2} \right), \tag{12b}$$

$$\mathcal{F}_{(u)}{}^{ab}{}_{a'b'}{}^{\{d\}} = \left(Dd^{a}{}_{b'd} - Ff^{a}{}_{b'd} \right) \left(Dd^{bd}{}_{a'} + Ff^{bd}{}_{a'} \right), \quad \widehat{\Gamma}^{\{d\}}_{(u)1} = \frac{1}{f^2} \left(1 + \frac{(m_{a'} + m_d)(m_a + m_d)}{u - m_d^2} \right),$$
$$\widehat{\Gamma}^{\{d\}}_{(u)0} = \frac{1}{f^2} \left(m_d - (m_{a'} + m_a - m_d) \frac{(m_{a'} + m_d)(m_a + m_d)}{u - m_d^2} \right). \tag{12c}$$

Here f is the pseudoscalar-meson decay constant in the chiral limit. The coupling constants D and F have been obtained from experimental data on hyperon semileptonic decays in [22, 23, 24]. The amplitudes (12) are obtained by resumming mass terms from the $\mathcal{O}(q^2)$ Lagrangian and incorporating them into the $\mathcal{O}(q^1)$ free baryon Lagrangian, thereby explicitly taking into account baryon mass splittings. This procedure is not inconsistent at leading order in the chiral expansion provided the result is not used as the basis of a next-to-leading order calculation. The purely leading-order result, however, can be trivially recovered from (12) by setting $m_a = M_\chi$ for all $a = 1, \ldots, 8$ in our expressions.

If we set in (12) all baryon masses to their chiral-limit common value M_χ, expand the Dirac spinors $\overline{u}'(p', \sigma')$ and $u(p, \sigma)$ into their upper and lower components, and change the flavor basis to the Gell-Mann basis, we recover the tree-level amplitudes of [25]. Furthermore, for those flavor coefficients considered in [26, 27] we find full numerical agreement with their tabulated values.

3 One-loop absorptive parts

The spin asymmetry (8) involves the absorptive part of the amplitude, which vanishes at tree level for physical values of the external momenta. At one-loop level the only diagrams that contribute to the absorptive part in

[2] $\mathcal{O}(q^n)$ denotes a generic quantity of chiral order n, with q a nominally small quantity such as a meson momentum or mass.
[3] Those flavor indices are arbitrarily written as upper indices, but between braces to denote their non-tensorial nature.

the physical region are those that can be factored as products of tree-level diagrams with on-shell external legs [28]. From (3), (4), (5) we have $\overline{u}'(p',\sigma')\Gamma_A{}^{ab}{}_{a'b'}\,u(p,\sigma) = 1/(2i)\langle B_{a'}(p',\sigma')M_{b'}(q')|(T-T^\dagger)|B^a(p,\sigma)M^b(q)\rangle$. Hence, from the unitarity relation $T - T^\dagger = i(2\pi)^4\delta(P_f - P_i)TT^\dagger$ we obtain the cutting rules for one-loop diagrams,

$$\overline{u}'(p',\sigma')\Gamma_A{}^{ab}{}_{a'b'}\,u(p,\sigma) = \frac{1}{8\pi^2}\int d^4Q d^4R\,\delta(p_{_T}-Q-R)\sum_{h,h'}\delta_+(Q^2-\widetilde{m}_{h'}^2)\delta_+(R^2-m_h^2) \times \overline{u}'(p',\sigma')\Gamma^{hh'}{}_{a'b'}(\not{R}+m_h)\overline{\Gamma}^{ab}{}_{hh'}\,u(p,\sigma). \quad (13)$$

A diagrammatic representation of this equation is given in fig. 1. Notice that meson–meson vertices do not enter the absorptive part at this order. We introduce the notation

$$\int dV_R\,\left(\widehat{\Gamma}^{\{d'\}}_{(\mathcal{G}')0}+\widehat{\Gamma}^{\{d'\}}_{(\mathcal{G}')1}\not{p}_{_T}\right)(\not{R}+m_h)\left(\widehat{\Gamma}^{\{d\}}_{(\mathcal{G})0}+\widehat{\Gamma}^{\{d\}}_{(\mathcal{G})1}\not{p}_{_T}\right) \doteq \left(\widehat{\Gamma}^{\{dd'\}}_{(\mathcal{G}\mathcal{G}')0}+\widehat{\Gamma}^{\{dd'\}}_{(\mathcal{G}\mathcal{G}')1}\not{p}_{_T}\right), \quad (14)$$

where $\mathcal{G},\mathcal{G}' = c,s,u$ and the integration measure dV_R, whose dependence on m_h, $\widetilde{m}_{h'}$ is not explicitly shown in the notation, is defined in (1). Similarly, the dependence of $\widehat{\Gamma}^{\{d'\}}_{(\mathcal{G}')0,1}$ on $m_{a'}$, m_h and that of $\widehat{\Gamma}^{\{d\}}_{(\mathcal{G})0,1}$ on m_a, m_h are not explicitly indicated. More specifically, the reduced amplitudes $\widehat{\Gamma}^{\{d'\}}_{(\mathcal{G}')0,1}$ and $\widehat{\Gamma}^{\{d\}}_{(\mathcal{G})0,1}$ in (14) correspond to the amplitudes $\langle B_{a'}(p',\sigma')M_{b'}(q')|T|B^h(R,\Sigma)M^{h'}(Q)\rangle$ and $\langle B_h(R,\Sigma)M_{h'}(Q)|T|B^a(p,\sigma)M^b(q)\rangle$, resp., evaluated at tree level. They are given by (12), with the appropriate changes in flavor, momentum, and spin variables. With (11) and (14), we can rewrite (13) in the more compact form

$$\Gamma_A{}^{ab}{}_{a'b'} \doteq \sum_{\mathcal{G},\mathcal{G}'}\sum_{h,h',d,d'}\mathcal{F}_{(\mathcal{G}')}{}^{hh'}{}_{a'b'}{}^{\{d'\}}\mathcal{F}_{(\mathcal{G})}{}^{ab}{}_{hh'}{}^{\{d\}}\frac{1}{8\pi^2}\left(\widehat{\Gamma}^{\{dd'\}}_{(\mathcal{G}\mathcal{G}')0}+\widehat{\Gamma}^{\{dd'\}}_{(\mathcal{G}\mathcal{G}')1}\not{p}_{_T}\right), \quad (15)$$

In (14) and (15), if $\mathcal{G}$ or $\mathcal{G}' = c$ the respective superindex d or d' must be omitted, since there are no internal particles propagating in the contact diagram.

3.1 Bubble diagrams

In those terms on the r.h.s. of (15) not involving $\mathcal{G}$ or $\mathcal{G}' = u$ the reduced form factors $\widehat{\Gamma}_{(\mathcal{G})0,1}$ and $\widehat{\Gamma}_{(\mathcal{G}')0,1}$ are independent of R^μ, so the integration is trivial. For those terms we have

$$\begin{aligned}
&\widehat{\Gamma}^{\{dd'\}}_{(\mathcal{G}\mathcal{G}')0} = sB_1^{\{hh'\}}H^{\{dd'\}}_{(\mathcal{G}\mathcal{G}')} + m_hB_0^{\{hh'\}}K^{\{dd'\}}_{(\mathcal{G}\mathcal{G}')}\ , \quad \widehat{\Gamma}^{\{dd'\}}_{(\mathcal{G}\mathcal{G}')1} = m_hB_0^{\{hh'\}}H^{\{dd'\}}_{(\mathcal{G}\mathcal{G}')} + B_1^{\{hh'\}}K^{\{dd'\}}_{(\mathcal{G}\mathcal{G}')}\ ,\\
&H^{\{dd'\}}_{(\mathcal{G}\mathcal{G}')} = \widehat{\Gamma}^{\{d'\}}_{(\mathcal{G}')0}\widehat{\Gamma}^{\{d\}}_{(\mathcal{G})1} + \widehat{\Gamma}^{\{d'\}}_{(\mathcal{G}')1}\widehat{\Gamma}^{\{d\}}_{(\mathcal{G})0}\ , \qquad K^{\{dd'\}}_{(\mathcal{G}\mathcal{G}')} = \widehat{\Gamma}^{\{d'\}}_{(\mathcal{G}')0}\widehat{\Gamma}^{\{d\}}_{(\mathcal{G})0} + s\widehat{\Gamma}^{\{d'\}}_{(\mathcal{G}')1}\widehat{\Gamma}^{\{d\}}_{(\mathcal{G})1}\ ,
\end{aligned} \quad (16)$$

with $\mathcal{G},\mathcal{G}' = c,s$. The phase-space integrals $B_{0,1}^{\{hh'\}}$ are given in B. The quantities $H^{\{dd'\}}_{(\mathcal{G}\mathcal{G}')}$ and $K^{\{dd'\}}_{(\mathcal{G}\mathcal{G}')}$ are introduced here for notational convenience. As with $\widehat{\Gamma}^{\{d\}}_{(\mathcal{G})0,1}$ and $\widehat{\Gamma}^{\{d'\}}_{(\mathcal{G}')0,1}$, their dependence on a, a', h, h' through initial and final state masses is not indicated explicitly for simplicity.

From (12) and the second line of (16) we have,

$$
\begin{aligned}
f^4 H_{(cc)} &= -\frac{1}{2}(m_a + m_{a'} + 2m_h)\ , & f^4 K_{(cc)} &= s + \frac{1}{4}(m_a + m_h)(m_{a'} + m_h),\\
f^4 H^{\{d'\}}_{(cs)} &= (m_{a'} + m_h) + \frac{1}{2}(m_a + m_h + 2m_{d'})\left(1 + \frac{(m_{a'} + m_{d'})(m_h + m_{d'})}{s - m_{d'}^2}\right),\\
f^4 K^{\{d'\}}_{(cs)} &= -\frac{1}{2}(m_{a'} + m_h)(m_a + m_h) - \left(s + \frac{m_{d'}}{2}(m_a + m_h)\right)\left(1 + \frac{(m_{a'} + m_{d'})(m_h + m_{d'})}{s - m_{d'}^2}\right),\\
H^{\{d\}}_{(sc)} &= H^{\{d\}}_{(cs)}\Big|_{a\leftrightarrow a'}\ , & K^{\{d\}}_{(sc)} &= K^{\{d\}}_{(cs)}\Big|_{a\leftrightarrow a'}\ ,\\
f^4 H^{\{dd'\}}_{(ss)} &= -\left(1 + \frac{(m_h + m_d)(m_a + m_d)}{s - m_d^2}\right)(m_{a'} + m_h) - \left(1 + \frac{(m_h + m_{d'})(m_{a'} + m_{d'})}{s - m_{d'}^2}\right)\\
&\quad \times (m_a + m_h) - (m_d + m_{d'})\left(1 + \frac{(m_h + m_d)(m_a + m_d)}{s - m_d^2}\right)\left(1 + \frac{(m_h + m_{d'})(m_{a'} + m_{d'})}{s - m_{d'}^2}\right),\\
f^4 K^{\{dd'\}}_{(ss)} &= (m_h + m_{a'})(m_h + m_a) + m_d(m_h + m_{a'})\left(1 + \frac{(m_h + m_d)(m_a + m_d)}{s - m_d^2}\right)\\
&\quad + m_{d'}(m_h + m_a)\left(1 + \frac{(m_h + m_{d'})(m_{a'} + m_{d'})}{s - m_{d'}^2}\right)\\
&\quad + (s + m_d m_{d'})\left(1 + \frac{(m_h + m_d)(m_a + m_d)}{s - m_d^2}\right)\left(1 + \frac{(m_h + m_{d'})(m_{a'} + m_{d'})}{s - m_{d'}^2}\right).
\end{aligned}
\tag{17}
$$

The contributions to the absorptive part (15) of the one-loop amplitude from diagrams (cc), (cs), (sc), (ss) (see fig. 1) is then given by (16) and (17).

3.2 Triangle diagrams

The terms in (15) for which $\mathcal{G}' = u \neq \mathcal{G}$ and those with $\mathcal{G}' \neq u = \mathcal{G}$ are almost identical. We will consider the former case first and then apply the results to the latter. For the diagrams (cu), (su) in fig. 1 the last factor in the integrand in (14) is independent of R^μ. Their contribution to (15) is then of the form

$$
\widehat{\Gamma}^{\{dd'\}}_{(\mathcal{G}u)0} = \Omega^{\{d'\}}_{(u_f)0}\widehat{\Gamma}^{\{d\}}_{(\mathcal{G})0} + s\Omega^{\{d'\}}_{(u_f)1}\widehat{\Gamma}^{\{d\}}_{(\mathcal{G})1}\ , \qquad \widehat{\Gamma}^{\{dd'\}}_{(\mathcal{G}u)1} = \Omega^{\{d'\}}_{(u_f)0}\widehat{\Gamma}^{\{d\}}_{(\mathcal{G})1} + \Omega^{\{d'\}}_{(u_f)1}\widehat{\Gamma}^{\{d\}}_{(\mathcal{G})0}\ , \tag{18}
$$

with $\Omega^{\{d'\}}_{(u_f)0,1}$ defined by the relation

$$
\int dV_R \left(\widehat{\Gamma}^{\{d'\}}_{(u)0} + \widehat{\Gamma}^{\{d'\}}_{(u)1}\not{p}_T\right)(\not{R} + m_h) \doteq \Omega^{\{d'\}}_{(u_f)0} + \Omega^{\{d'\}}_{(u_f)1}\not{p}_T\ . \tag{19}
$$

In order to obtain $\Omega^{\{d'\}}_{(u_f)0,1}$ we further split (19) as

$$
\Omega^{\{d'\}}_{(u_f)0} = \Omega^{\{d'\}}_{(u_f)00} + \Omega^{\{d'\}}_{(u_f)10}\ , \qquad \Omega^{\{d'\}}_{(u_f)1} = \Omega^{\{d'\}}_{(u_f)01} + \Omega^{\{d'\}}_{(u_f)11}\ , \tag{20a}
$$

$$
\int dV_R \widehat{\Gamma}^{\{d'\}}_{(u)0}(\not{R} + m_h) \doteq \Omega^{\{d'\}}_{(u_f)00} + \Omega^{\{d'\}}_{(u_f)01}\not{p}_T\ , \quad \int dV_R \widehat{\Gamma}^{\{d'\}}_{(u)1}\not{p}_T(\not{R} + m_h) \doteq \Omega^{\{d'\}}_{(u_f)10} + \Omega^{\{d'\}}_{(u_f)11}\not{p}_T\ . \tag{20b}
$$

The integrals in (20b) can be evaluated in terms of the bubble and triangle integrals of B. Terms proportional to $\not{q}'$ and $\not{p}_T\not{q}'$, coming from $\not{C}_1^{(u_f)}$ and $\not{p}_T\not{C}_1^{(u_f)}$, reduce to the form (20b) when sandwiched between $\overline{u}'$ and u, since $\not{q}' \doteq \not{p}_T - m_{a'}$ and $\not{p}_T\not{q}' \doteq m_{a'}\not{p}_T - m_{a'}^2 + \widetilde{m}_{b'}^2$. This yields the result,

$$
\begin{aligned}
f^4\Omega^{\{d'\}}_{(u_f)00} &= m_{d'}m_h B_0^{hh'} - (m_h + m_{a'} - m_{d'})(m_h + m_{d'})(m_{a'} + m_{d'})\left(m_h C_0^{(u_f)} - m_{a'}F_2^{(u_f)}\right),\\
f^4\Omega^{\{d'\}}_{(u_f)01} &= m_{d'}B_1^{hh'} - (m_h + m_{a'} - m_{d'})(m_h + m_{d'})(m_{a'} + m_{d'})\left(F_1^{(u_f)} + F_2^{(u_f)}\right),\\
f^4\Omega^{\{d'\}}_{(u_f)10} &= sB_1^{hh'} + (m_h + m_{d'})(m_{a'} + m_{d'})\left(sF_1^{(u_f)} - (m_{a'}^2 - \widetilde{m}_{b'}^2)F_2^{(u_f)}\right),\\
f^4\Omega^{\{d'\}}_{(u_f)11} &= m_h B_0^{hh'} + (m_h + m_{d'})(m_{a'} + m_{d'})\left(m_{a'}F_2^{(u_f)} + m_h C_0^{(u_f)}\right).
\end{aligned}
\tag{21}
$$

The contribution of diagrams cu, su to the absorptive part of the amplitude, given by the terms in (15) with $\mathcal{G}' = u$ and $\mathcal{G} = c, s$, are then determined by (18), (20) and (21) in terms of the scalar integrals of B.

Similarly, the absorptive part of diagrams (uc), (us) is given by those terms in (15) with $\mathcal{G}' = c, s$ and $\mathcal{G} = u$. In this case we have,

$$\widehat{\Gamma}^{\{dd'\}}_{(u\mathcal{G}')0} = \Omega^{\{d\}}_{(u_i)0}\widehat{\Gamma}^{\{d'\}}_{(\mathcal{G}')0} + s\Omega^{\{d\}}_{(u_i)1}\widehat{\Gamma}^{\{d'\}}_{(\mathcal{G}')1} \ , \qquad \widehat{\Gamma}^{\{dd'\}}_{(u\mathcal{G}')1} = \Omega^{\{d\}}_{(u_i)0}\widehat{\Gamma}^{\{d'\}}_{(\mathcal{G}')1} + \Omega^{\{d\}}_{(u_i)1}\widehat{\Gamma}^{\{d'\}}_{(\mathcal{G}')0} \ . \tag{22}$$

The form factors $\Omega^{\{d\}}_{(u_i)0,1}$, defined by the analog of (19)

$$\int dV_R(\not{R} + m_h)\left(\widehat{\Gamma}^{\{d\}}_{(u)0} + \widehat{\Gamma}^{\{d\}}_{(u)1}\not{p}_T\right) \doteq \Omega^{\{d\}}_{(u_i)0} + \Omega^{\{d\}}_{(u_i)1}\not{p}_T \ , \tag{23}$$

are given by (20a) and (21) with the substitutions $(u_f) \to (u_i)$, $a' \to a$, $b' \to b$, $d' \to d$ in terms of the scalar integrals $C_0^{(u_i)}$, $F_1^{(u_i)}$, $F_2^{(u_i)}$ given in B.

3.3 Box diagram

The term in (15) with $\mathcal{G} = u = \mathcal{G}'$ is of the form,

$$\widehat{\Gamma}^{\{dd'\}}_{(uu)k} = \sum_{i,j=0}^{1} \Omega^{\{dd'\}}_{(ij)k} \ , \qquad k = 0, 1 \ , \tag{24}$$

where $\Omega^{\{dd'\}}_{(ij)0,1}$, $i, j = 0, 1$, are defined by the relations

$$\begin{aligned}
\int dV_R \widehat{\Gamma}^{\{d'\}}_{(u)0}\widehat{\Gamma}^{\{d\}}_{(u)0}(\not{R} + m_h) &\doteq \Omega^{\{dd'\}}_{(00)0} + \Omega^{\{dd'\}}_{(00)1}\not{p}_T \ , \\
\int dV_R \widehat{\Gamma}^{\{d'\}}_{(u)0}\widehat{\Gamma}^{\{d\}}_{(u)1}(\not{R} + m_h)\not{p}_T &\doteq \Omega^{\{dd'\}}_{(01)0} + \Omega^{\{dd'\}}_{(01)1}\not{p}_T \ , \\
\int dV_R \widehat{\Gamma}^{\{d'\}}_{(u)1}\widehat{\Gamma}^{\{d\}}_{(u)0}\not{p}_T(\not{R} + m_h) &\doteq \Omega^{\{dd'\}}_{(10)0} + \Omega^{\{dd'\}}_{(10)1}\not{p}_T \ , \\
\int dV_R \widehat{\Gamma}^{\{d'\}}_{(u)1}\widehat{\Gamma}^{\{d\}}_{(u)1}\not{p}_T(\not{R} + m_h)\not{p}_T &\doteq \Omega^{\{dd'\}}_{(11)0} + \Omega^{\{dd'\}}_{(11)1}\not{p}_T \ .
\end{aligned} \tag{25}$$

Direct evaluation of these integrals, and use of the Dirac equation in the form $\not{q}\not{p}_T \doteq m_a\not{p}_T - m_a^2 + \widetilde{m}_b^2$, $\not{p}_T\not{q}'\not{p}_T \doteq m_{a'}s - (m_{a'}^2 - \widetilde{m}_{b'}^2)\not{p}_T$, etc., leads to,

$$\begin{aligned}
f^4\Omega^{\{dd'\}}_{(00)0} &= m_d m_{d'} m_h B_0^{\{hh'\}} + m_{d'}(m_a + m_h - m_d)(m_h + m_d)(m_a + m_d)\left[m_a F_2^{(u_i)} - m_h C_0^{(u_i)}\right] \\
&\quad + m_d(m_{a'} + m_h - m_{d'})(m_h + m_{d'})(m_{a'} + m_{d'})\left[m_{a'} F_2^{(u_f)} - m_h C_0^{(u_f)}\right] \\
&\quad + (m_{a'} + m_h - m_{d'})(m_h + m_{d'})(m_{a'} + m_{d'})(m_a + m_h - m_d)(m_h + m_d)(m_a + m_d) \\
&\quad \times \left[-m_a F_2^{(uu)} - m_{a'} F_3^{(uu)} + m_h D_0\right], \\
f^4\Omega^{\{dd'\}}_{(00)1} &= m_d m_{d'} B_1^{\{hh'\}} - m_{d'}(m_a + m_h - m_d)(m_h + m_d)(m_a + m_d)\left[F_1^{(u_i)} + F_2^{(u_i)}\right] \\
&\quad - m_d(m_{a'} + m_h - m_{d'})(m_h + m_{d'})(m_{a'} + m_{d'})\left[F_1^{(u_f)} + F_2^{(u_f)}\right] \\
&\quad + (m_{a'} + m_h - m_{d'})(m_h + m_{d'})(m_{a'} + m_{d'})(m_a + m_h - m_d)(m_h + m_d)(m_a + m_d) \\
&\quad \times \left[F_1^{(uu)} + F_2^{(uu)} + F_3^{(uu)}\right], \\
f^4\Omega^{\{dd'\}}_{(01)0} &= m_{d'} s B_1^{\{hh'\}} + m_{d'}(m_h + m_d)(m_a + m_d)\left[sF_1^{(u_i)} - (m_a^2 - \widetilde{m}_b^2)F_2^{(u_i)}\right] \\
&\quad - s(m_{a'} + m_h - m_{d'})(m_h + m_{d'})(m_{a'} + m_{d'})\left[F_1^{(u_f)} + F_2^{(u_f)}\right]
\end{aligned}$$

$$
\begin{aligned}
&- (m_{a'} + m_h - m_{d'})(m_h + m_{d'})(m_{a'} + m_{d'})(m_h + m_d)(m_a + m_d) \\
&\times \left[s F_1^{(uu)} - (m_a^2 - \widetilde{m}_b^2) F_2^{(uu)} + s F_3^{(uu)} \right], \\
f^4 \Omega_{(01)1}^{\{dd'\}} &= m_{d'} m_h B_0^{\{hh'\}} + m_{d'}(m_h + m_d)(m_a + m_d) \left[m_h C_0^{(u_i)} + m_a F_2^{(u_i)} \right] \\
&- (m_{a'} + m_h - m_{d'})(m_h + m_{d'})(m_{a'} + m_{d'}) \left[m_h C_0^{(u_f)} - m_{a'} F_2^{(u_f)} \right] \\
&- (m_{a'} + m_h - m_{d'})(m_h + m_{d'})(m_{a'} + m_{d'})(m_h + m_d)(m_a + m_d) \\
&\times \left[m_h D_0 + m_a F_2^{(uu)} - m_{a'} F_3^{(uu)} \right], \\
f^4 \Omega_{(10)0}^{\{dd'\}} &= m_d s B_1^{\{hh'\}} + m_d(m_h + m_{d'})(m_{a'} + m_{d'}) \left[s F_1^{(u_f)} - (m_{a'}^2 - \widetilde{m}_{b'}^2) F_2^{(u_f)} \right] \\
&- s(m_a + m_h - m_d)(m_h + m_d)(m_a + m_d) \left[F_1^{(u_i)} + F_2^{(u_i)} \right] \\
&- (m_a + m_h - m_d)(m_h + m_{d'})(m_{a'} + m_{d'})(m_h + m_d)(m_a + m_d) \\
&\times \left[s F_1^{(uu)} + s F_2^{(uu)} - (m_{a'}^2 - \widetilde{m}_{b'}^2) F_3^{(uu)} \right], \\
f^4 \Omega_{(10)1}^{\{dd'\}} &= m_d m_h B_0^{\{hh'\}} + m_d(m_h + m_{d'})(m_{a'} + m_{d'}) \left[m_h C_0^{(u_f)} + m_{a'} F_2^{(u_f)} \right] \\
&- (m_a + m_h - m_d)(m_h + m_d)(m_a + m_d) \left[m_h C_0^{(u_i)} - m_a F_2^{(u_i)} \right] \\
&- (m_a + m_h - m_d)(m_h + m_{d'})(m_{a'} + m_{d'})(m_h + m_d)(m_a + m_d) \\
&\times \left[m_h D_0 - m_a F_2^{(uu)} + m_{a'} F_3^{(uu)} \right], \\
f^4 \Omega_{(11)0}^{\{dd'\}} &= s m_h B_0^{\{hh'\}} + (m_h + m_d)(m_a + m_d) s \left[m_h C_0^{(u_i)} + m_a F_2^{(u_i)} \right] \\
&+ (m_h + m_{d'})(m_{a'} + m_{d'}) s \left[m_h C_0^{(u_f)} + m_{a'} F_2^{(u_f)} \right] \\
&+ (m_h + m_{d'})(m_{a'} + m_{d'})(m_h + m_d)(m_a + m_d) s \left[m_h D_0 + m_a F_2^{(uu)} + m_{a'} F_3^{(uu)} \right], \\
f^4 \Omega_{(11)1}^{\{dd'\}} &= s B_1^{\{hh'\}} + (m_h + m_d)(m_a + m_d) \left[s F_1^{(u_i)} - (m_a^2 - \widetilde{m}_b^2) F_2^{(u_i)} \right] \\
&+ (m_h + m_{d'})(m_{a'} + m_{d'}) \left[s F_1^{(u_f)} - (m_{a'}^2 - \widetilde{m}_{b'}^2) F_2^{(u_f)} \right] \\
&+ (m_h + m_{d'})(m_{a'} + m_{d'})(m_h + m_d)(m_a + m_d) \\
&\times \left[s F_1^{(uu)} - (m_a^2 - \widetilde{m}_b^2) F_2^{(uu)} - (m_{a'}^2 - \widetilde{m}_{b'}^2) F_3^{(uu)} \right]. \qquad (26)
\end{aligned}
$$

Thus, the contribution to (15) from the box diagram (uu) in fig. 1 is given by (24) and (26) in terms of the scalar integrals of B.

4 Discussion: numerical results

The expression (10) for the polarization involves the tree-level scattering amplitude (12), and the absorptive part of the one-loop amplitude as given explicitly in analytical form in sect. 3 and B. In this section we discuss those results from a numerical point of view.

For numerical computations we use physical meson and baryon masses, and coupling constants $D = 0.80 \pm 0.01$ and $F = 0.46 \pm 0.01$ [22] (see also [23, 24]). The meson weak-decay constant f should be given, in principle, its chiral-limit value $f_0 < f_\pi$ which in SU(3) chiral perturbation theory is not precisely known (see [25] and refs. cited there). Since we are working at leading order we can, alternatively, set f to an average of its physical values $\langle f_{\pi,K,\eta} \rangle > f_\pi$. Both possibilities have been used in phenomenological analyses in the framework of Unitarized Baryon Chiral Perturbation Theory (UBChPT). Data on meson–baryon scattering cross sections and threshold branching fractions have been succesfully described in UBChPT with $f \cong 74$—86 MeV [25], and with $f = 1.123 f_\pi \cong 103$ MeV [26, 27, 29]. In numerical computations we adopt

the latter value, and discuss the dependence on f of our results below.

If we restrict ourselves strictly to leading-order perturbation theory the denominator in (10) must be $|\mathcal{T}_{\rm tree}|^2$. The polarization $\mathcal{P}'_{*\rm l.o.}$ computed in this way satisfies $|\mathcal{P}'_{*\rm l.o.}| \leq 1$ only perturbatively. That inequality can be violated if the one-loop absorptive amplitude entering the asymmetry $\mathcal{A}'_*$ in the numerator of (10) is not much smaller than the tree-level amplitude $\mathcal{T}_{\rm tree}$, thus signalling a breakdown of the l.o. approximation. We denote $\mathcal{P}'_*$ the polarization computed using the same amplitude $\mathcal{T} = \mathcal{T}_{\rm tree} + i\mathcal{T}_{1-\rm loop,abs.}$ in the denominator of (10) as in the numerator, so that $|\mathcal{P}'_*| \leq 1$ holds exactly. We may consider the difference of $\mathcal{P}'_*$ and $\mathcal{P}'_{*\rm l.o.}$ as a rough measure of the validity of the l.o. approximation for the polarization. From (12) and fig. 1 we find that $\mathcal{T}_{\rm tree} \propto 1/f^2$, $\mathcal{T}_{1-\rm loop,abs.} \propto 1/f^4$, and $\mathcal{A} \propto 1/f^6$. Therefore, $\mathcal{P}'_{*\rm l.o.} \propto 1/f^2$ and $\mathcal{P}'_* \sim 1/(c_1 f^2 + c_2 + c_3/f^2)$, with $c_{1,2,3}$ some f-independent coefficients. Thus, the difference $|\mathcal{P}'_* - \mathcal{P}'_{*\rm l.o.}|$ is expected to increase with decreasing f. In those processes and kinematic regions where the l.o. approximation is accurate we expect both $\mathcal{P}'_{*\rm l.o.}$ and $\mathcal{P}'_*$ to scale with f as $1/f^2$, the former exactly and the latter approximately.

In figs. 2—5 we plot the polarization $\mathcal{P}'_*$ as a function of the center-of-mass scattering angle for several reactions and values of $\sqrt{s}$, as an illustration of the results obtained in the previous sections directly from BChPT. $\mathcal{P}'_{*\rm l.o.}$ is also shown in those figures for comparison.

For $p\pi^\pm \to p\pi^\pm$ and $p\pi^- \to n\pi^0$, curves (1)–(3) in fig. 2 correspond to energies more than 100 MeV below the Δ-resonance peak, in the region where BChPT should be applicable. $\mathcal{P}'_*$ and $\mathcal{P}'_{*\rm l.o.}$ do not differ appreciably at those energies, except for curve (3) for $p\pi^- \to p\pi^-$, pointing to a good convergence of perturbation theory in that energy region. As seen in the figure, $\mathcal{P}'_*$ reaches sizable values for the elastic processes. For $q_{\rm lab} \gtrsim 100$ MeV not only higher-order corrections are expected to become important, but also the Δ resonance contributions are essential. In fig. 3 we plot the polarization $\mathcal{P}'_*$ including the contribution from the pole in s-channel Δ resonance exchange. The latter, not contained in our analytical results, was computed numerically from the scattering amplitudes in [30]. As seen from the figure, the Δ resonance contribution to $\mathcal{P}'_*$ is already quantitatively significant at $q_{\rm lab} = 125$ MeV, becoming the dominant one at higher energies. As expected, within the resonance peak our analytical results are not applicable.

Our results for $pK^+ \to pK^+$ are shown in fig. 4. For this process we expect BChPT to be valid over the entire energy range of the figure, whose highest $\sqrt{s}$ is about 250 MeV below the $\Delta^{++}K^0/\Delta^+K^+$ rest mass at the Δ peak. The difference of $\mathcal{P}'_*$ and $\mathcal{P}'_{*\rm l.o.}$ is large for curve (6) in fig. 4, reflecting the fact that higher-order corrections become important at about $q_{\rm lab} \sim 300$ MeV. As seen in the figures, the polarizations $\mathcal{P}'_*$ in $p\pi^+ \to p\pi^+$ and $pK^+ \to pK^+$ are in relation $(\mathcal{P}'_*)_{p\pi^+} \sim 10(\mathcal{P}'_*)_{pK^+}$ at fixed initial meson momentum and $-1 < \cos\theta_{\rm cm} < 1$. This fact deserves some consideration since we expect the dynamics to be similar in both elastic processes, except for the stronger coupling in the $S = 1$ channel due to the larger kaon mass.[4] Restricting ourselves to $0 \leq q_{\rm lab} \leq 125$ MeV where the difference between $|\mathcal{T}|^2$ and $|\mathcal{T}_{\rm tree}|^2$ is negligible, for the spin asymmetry $\mathcal{A}'_*$ defined in (8) and (9) numerically we find, roughly, $(\mathcal{A}'_*)_{p\pi^+} \sim 1/10(\mathcal{A}'_*)_{pK^+}$. The factor $|\vec{q} \wedge \vec{p}|$ in (9) is almost equal in both processes. Whereas in $p\pi^+$ elastic scattering the two terms in the factor $({\rm Re}\Gamma_0{\rm Im}\Gamma_1 - {\rm Im}\Gamma_0{\rm Re}\Gamma_1)$ in (8) partially cancel, in pK^+ they have the same sign, leading to a larger spin asymmetry for the latter process.[5] From (7), $|\mathcal{T}|^2$ is a sum of three terms $C\Gamma^2$ which, for each of the two processes, are all of the same order of magnitude. Numerically, we have $(C\Gamma^2)_{p\pi^+} \sim 10(C\Gamma^2)_{pK^+}$ [6] which suggests an analogous relation holds for $|\mathcal{T}|^2$, therefore apparently leading to the wrong result $(\mathcal{P}'_*)_{p\pi^+} \sim 1/100(\mathcal{P}'_*)_{pK^+}$. In fact, due to destructive interference between the spin-flip and non-spin-flip terms in the tree-level amplitude, we have $|\mathcal{T}|^2_{pK^+} \sim 1/10(C\Gamma^2)_{pK^+}$ and a much stronger effect in $p\pi^+$, $|\mathcal{T}|^2_{p\pi^+} \sim 1/10^4(C\Gamma^2)_{p\pi^+}$. Therefore, we get $|\mathcal{T}|^2_{p\pi^+} \sim 1/10^2|\mathcal{T}|^2_{pK^+}$ which, together with the above relation for $\mathcal{A}'_*$, results in $(\mathcal{P}'_*)_{p\pi^+} \sim 10(\mathcal{P}'_*)_{pK^+}$.

Due to the strong coupling in the $S = -1$ sector [6, 25, 26, 31] BChPT is not directly applicable to nucleon–antikaon processes. Rather, higher-order corrections must be resummed with unitarization techniques such as UBChPT. In the $I = 0$ channels the $\Lambda(1405)$ resonance lies $\sim$25 MeV below threshold, domi-

[4] Notice that for both $p\pi$ interactions in the $I = 3/2$ sector and pK with $I = 1$ the scattering lengths are negative, indicating a repulsive interaction [7].

[5] The crucial sign difference between the two elastic processes comes from ${\rm Im}\Gamma_1$.

[6] The factors C_{ij} in (7) are essentially equal for the two elastic processes. The factor ~ 10 referred to here comes from the squared tree-level amplitudes. Specifically, the u-channel contribution in pK^+ scattering is smaller than in $p\pi^+$, and that of the c-channel is almost equal for both processes.

nating the dynamics of $pK^- \to \Sigma\pi$ near threshold in the S wave. In the $I = 1$ channels $pK^- \to \Lambda\pi^0, \Sigma\pi$ the narrow decuplet $\Sigma(1385)$ lies $\sim$46 MeV below threshold. The effect on final-state polarization of such strong-coupling phenomena, not taken into account in this paper, will be discussed elsewhere. For completitude, however, we illustrate our BChPT results for $\mathcal{P}'_*$ for several pK^- scattering processes in fig. 5, about which we shall make some qualitative remarks. As seen there, the difference of $\mathcal{P}'_*$ and $\mathcal{P}'_{*\mathrm{l.o.}}$ is relatively small in the $\Lambda\pi^0$ channel but very large in the $\Sigma^-\pi^+$ channel, where $|\mathcal{P}'_{*\mathrm{l.o.}}| > 1$ over most of the range of $\cos\theta_{\mathrm{cm}}$, whereas the other two channels are intermediate between those cases, with large $|\mathcal{P}'_* - \mathcal{P}'_{*\mathrm{l.o.}}|$ but $|\mathcal{P}'_{*\mathrm{l.o.}}| < 1$. Such large contributions from the one-loop absorptive part signal the inapplicability of perturbation theory. The sign of $\mathcal{P}'_*$ in the $\Sigma^-\pi^+$ channel is opposite to that of the other channels, and the maximum of $|\mathcal{P}'_*|$ over the range $-1 \le \cos\theta_{\mathrm{cm}} \le 1$ shows a much weaker dependence on energy in that channel than in the others.

5 Final Remarks

In this paper we computed the spin asymmetry and the polarization for the final-state baryon in unpolarized two-body meson–baryon scattering in lowest non-trivial order BChPT. The spin asymmetry (8) is a purely quantum effect which arises from the interference of the spin-flip and non-spin-flip amplitudes when on-shell intermediate channels are open. More precisely, the asymmetry is proportional to $\mathrm{Im}(\Gamma_0\Gamma_1^*)$, which must vanish if the imaginary parts of both factors are zero as happens at tree level. The expression (8) for $\mathcal{A}$ is a direct consequence of the form (3a) of the amplitude, which in turn follows from Lorentz covariance, the discrete spacetime symmetries of the strong interactions, and the spin and parity quantum numbers of ground-state mesons and baryons.

The scattering amplitudes are computed above in a physical flavor basis, incorporating baryon mass splittings already in the tree-level expressions (12). As mentioned in Sect. 2.1, including higher-order flavor-breaking effects is not inconsistent at leading order. The necessary absorptive parts are obtained at one-loop level from the purely dispersive tree-level amplitudes by means of unitarity relations. Those are given in Sect. 3 and in B in closed analytical form, a result which is interesting by itself due to its applicability in other perturbative computations.

A numerical analysis of our results for the spin asymmetry and polarization is carried out in Sect. 4, where several meson–proton processes are considered. Polarization effects are seen there to become stronger the higher the energy of the process. Yet, even at the very low energies above threshold at which BChPT can reasonably be expected to be applicable, sizable values of polarization are found in some processes, both in elastic and inelastic reaction channels. In elastic $N\pi$ scattering polarizations in the range $\sim$ 10—25% are found. By contrast, for the reasons analyzed above, polarizations for $pK^+ \to pK^+$ are smaller. In the $S = -1$ meson–baryon sector the leading-order approximation used here cannot be expected to be valid. In fact, it is known that due to the strong coupling and subthreshold resonances ($\Lambda(1405)$) in this sector, non-perturbative coupled-channels analysis are required to reproduce available cross-section data. The polarization curves in fig. 5 are only meant to illustrate the leading-order results obtained here for the polarization.

As discussed in sect. 4, a source of uncertainty in the leading-order result is the value of f. That uncertainty is inherent in the leading-order approximation, since it is higher-order corrections that shift f from its chiral-limit value and split it into its physical values. On the other hand, the chiral-limit f is subject to considerable uncertainty itself in the three-flavor case. The effects of a variation in f on our results are readily quantifiable, however, since we expect the polarization to scale approximately as $1/f^2$ (and exactly so at leading order). We remark that the numerical value for f used in sect. 4 is conservative in this respect, with lower values of f resulting in polarizations larger (up to a factor of about 2 for f as low as 76 MeV) than those reported in figs. 2—5.

Finally, we hope that the results obtained here may prompt a re-analysis of the wealth of data obtained in many experiments with meson beams (π beams at LAMPF, TRIUMF and PSI, for instance) in the past decades, leading to experimental information on the observables discussed here.

Acknowledgements

I would like to thank Prof. C. A. García Canal for his useful comments on a preliminary version of this paper.

References

[1] V. Bernard, U. G. Meissner, Annu. Rev. Nucl. Part. Sci. **57** (2007) 33.

[2] B. Borasoy, *Introduction to Chiral Perturbation Theory,* Lectures given at the 2nd Summer School on Particle Accelerators and Detectors, Bodrum, Turkey, Sep. 2006; arxiv:hep-ph/0703297.

[3] S. Scherer, M. R. Schindler, *A Chiral Perturbation Theory Primer,* lectures given at the European Centre for Theoretical Studies in Nuclear Physics and Related Areas, Trento, Italy, 2005; arxiv:hep-ph/0505265.

[4] S. Weinberg, *The Quantum Theory of Fields*, Vol. II, Cambridge Univ. Press, New York, 1996.

[5] J. F. Donoghue, E. Golowich, B. R. Holstein, *Dynamics of the Standard Model,* Cambridge Univ. Press, New York, 1994.

[6] V. Bernard, *Chiral Perturbation Theory and Baryon Properties,* arXiv:0706.0312.

[7] V. Bernard, N. Kaiser, U.-G. Meissner, Int. J. Mod. Phys. E **4** (1995) 193.

[8] E. Leader, *Spin in Particle Physics,* Cambridge Univ. Press, New York, 2001.

[9] M. E. Sevior et al., Phys. Rev. C **40** (1989) 2780.

[10] G. J. Hoffman et al., Phys. Rev. C **58** (1998) 3484.

[11] G. J. Hoffman et al., Phys. Rev. C **68** (2003) 018202.

[12] R. Wieser et al., Phys. Rev. C **54** (1996) 1930.

[13] R. Meier et al., Phys. Lett. B **588** (2004) 155.

[14] B. R. Lovett et al., Phys. Rev. D **23** (1981) 1924.

[15] J. Félix, Mod. Phys. Lett. A **14** (1999) 827.

[16] J. Gasser, M. E. Sainio, A. Svark, Nucl. Phys. **B 307** (1988) 779.

[17] J. Gasser, H. Leutwyler, Ann. Phys. (N.Y.) **158** (1984) 142.

[18] J. Gasser, H. Leutwyler, Nucl. Phys. B **250** (1985) 465.

[19] A. Krause, Helv. Phys. Acta **63** (1990) 3.

[20] M. Frink, U. G. Meissner, J. High Energy Phys. **0407** (2004) 028.

[21] J. A. Oller, J. Prades, M. Verbeni, J. High Energy Phys. **0609** (2006) 079, Erratum: arxiv:hep-ph/0701096.

[22] F. E. Close, R. G. Roberts, Phys. Lett. B **316** (1993) 165.

[23] B. Borasoy, Phys. Rev. D **59** (1999) 054021.

[24] P. G. Ratcliffe, Phys. Rev. D **59** (1999) 014038.

[25] J. A. Oller, U. G. Meissner, Phys. Lett. B **500** (2001) 263.

[26] E. Oset, A. Ramos, Nucl. Phys. A **635** (1998) 99.

[27] D. Jido, E. Oset, A. Ramos, Phys. Rev. C **66** (2002) 055203.

[28] S. Coleman, Nuov. Cim. **38** (1965) 438.

[29] E. Oset, A. Ramos, C. Bennhold, Phys. Lett. B **527** (2002) 99, Erratum: Phys. Lett. B **530** (2002) 260.

[30] U. G. Meissner, J. A. Oller, Nucl. Phys. A **673** (2000) 311.

[31] C.-H. Lee, H. Jung, D.-P. Min, M. Rho, Phys. Lett. B **326** (1994) 14.

[32] G. 't Hooft, M. Veltman, Nucl. Phys. B **153** (1979) 365.

[33] A. Denner, U. Nierste, R. Scharf, Nucl. Phys. B **367** (1991) 637.

[34] G. Passarino, M. Veltman, Nucl. Phys. B **160** (1979) 151.

[35] H. Schweinler, E. Wigner, J. Math. Phys. **11** (1970) 1693.

A Kinematics

In this appendix we gather some kinematical definitions used throughout the paper. We introduce the notation

$$\omega(x,y,z) = (x^2+y^2+z^2-2xy-2xz-2yz)^{\frac{1}{2}} = (x-(\sqrt{y}+\sqrt{z})^2)^{\frac{1}{2}}(x-(\sqrt{y}-\sqrt{z})^2)^{\frac{1}{2}} \ . \tag{27}$$

The function ω appears frequently in relativistic kinematics (*e.g.,* in the center of mass frame $|\vec{p}| = \omega(s, m_a^2, \widetilde{m}_b^2)/(2\sqrt{s})$). The Mandelstam invariants for the process $|B^a(p,\sigma)M^b(q)\rangle \longrightarrow |B^{a'}(p',\sigma')M^{b'}(q')\rangle$ are

$$s=(p+q)^2=(p'+q')^2 \ , \quad t=(p-p')^2=(q-q')^2 \ , \quad u=(p-q')^2=(p'-q)^2 \ , \tag{28}$$

with $s+t+u = m_a^2 + m_{a'}^2 + \widetilde{m}_b^2 + \widetilde{m}_{b'}^2$. The physical region for the process is defined by the inequalities

$$s_{\rm th} \le s \ , \quad t_{\rm min} \le t \le t_{\rm max} \ , \quad u_{\rm min} \le u \le u_{\rm max} \ , \tag{29}$$

where,

$$\begin{aligned}
s_{\rm th} &= \max\left\{(m_a+\widetilde{m}_b)^2, (m_{a'}+\widetilde{m}_{b'})^2\right\} \\
t_{\rm min}^{\rm max} &= -\frac{1}{2s}\left(s^2 - s(m_a^2+m_{a'}^2+\widetilde{m}_b^2+\widetilde{m}_{b'}^2) + (m_a^2-\widetilde{m}_b^2)(m_{a'}^2-\widetilde{m}_{b'}^2)\right) \\
&\quad \pm \frac{1}{2s}\omega(s,m_a^2,\widetilde{m}_b^2)\omega(s,m_{a'}^2,\widetilde{m}_{b'}^2), \\
u_{\rm min}^{\rm max} &= -\frac{1}{2s}\left(s^2 - s(m_a^2+m_{a'}^2+\widetilde{m}_b^2+\widetilde{m}_{b'}^2) - (m_a^2-\widetilde{m}_b^2)(m_{a'}^2-\widetilde{m}_{b'}^2)\right) \\
&\quad \pm \frac{1}{2s}\omega(s,m_a^2,\widetilde{m}_b^2)\omega(s,m_{a'}^2,\widetilde{m}_{b'}^2).
\end{aligned} \tag{30}$$

B Phase-space integrals

In this section we collect analytical results for some phase-space integrals. The notation we use is analogous to that for the loop integrals of which they are absorptive (or, for scalar integrals, imaginary) parts. The analytical expressions, obtained by standard methods [32, 33, 34], hold only in the physical region defined in (29). The volume element is in all cases

$$dV_R \equiv d^4R\,\delta_+(R^2-m_h^2)\delta_+((p_{_T}-R)^2-\widetilde{m}_{h'}^2), \tag{1}$$

where $\delta_+(x^2) \equiv \delta(x^2)\theta(x^0)$ for any (timelike) four-vector x^μ, with θ a unit step function.

B.1 Bubble diagrams

$$
\begin{aligned}
B_0^{\{hh'\}} &= \int dV_R\, 1 = \frac{\pi}{2}\frac{\omega(s, m_h^2, \widetilde{m}_{h'}^2)}{s}\theta(\sqrt{s} - m_h - \widetilde{m}_{h'}) \\
B_1^{\{hh'\}} &= \frac{1}{s}\int dV_R\, p_T \cdot R = \frac{s + m_h^2 - \widetilde{m}_{h'}^2}{2s} B_0^{\{hh'\}} \\
B_1^{\{hh'\}\mu} &= \int dV_R\, R^\mu = B_1^{\{hh'\}} p_T^\mu
\end{aligned}
\tag{2}
$$

B.2 Triangle diagrams

Integrals related to triangle diagrams are generically denoted by C. To avoid having to attach long lists of arguments to that symbol, we distinguish between diagrams in which the external particles directly attached to the trivalent vertices of the triangle are those of the final or of the initial state. In the former case integrals are denoted $C^{(u_f)}$, and in the latter $C^{(u_i)}$ (see fig. 6).

For integrals of type $C^{(u_f)}$ (diagrams *cu* and *su* in fig. 1) the integrand depends on $u_f = (R - q')^2$. The kinematic limits $u_{f\substack{\max\\\min}}$ for u_f are obtained from $u_{\substack{\max\\\min}}$ in (30) with the substitutions $a \to h$, $b \to h'$. The scalar integrals are,

$$
C_0^{(u_f)} = \int dV_R \frac{1}{u_f - m_{d'}^2} = -\frac{\pi}{2}\frac{\theta(\sqrt{s} - m_h - \widetilde{m}_{h'})}{\omega(s, m_{a'}^2, \widetilde{m}_{b'}^2)} \log\left(\frac{m_{d'}^2 - u_{f_{\min}}}{m_{d'}^2 - u_{f_{\max}}}\right) \tag{3}
$$

$$
C_{1p_T}^{(u_f)} = \int dV_R \frac{p_T \cdot R}{u_f - m_{d'}^2} = \frac{s + m_h^2 - \widetilde{m}_{h'}^2}{2} C_0^{(u_f)} \tag{4}
$$

$$
C_{1q'}^{(u_f)} = \int dV_R \frac{q' \cdot R}{u_f - m_{d'}^2} = \frac{1}{2}(m_h^2 + \widetilde{m}_{h'}^2 - m_{d'}^2) C_0^{(u_f)} - \frac{1}{2} B_0^{\{hh'\}} \tag{5}
$$

For the vector integral we introduce two sets of form factors, $G_{1,2}^{(u_f)}$ are obtained by orthogonal projection and algebraic reduction, and $F_{1,2}^{(u_f)}$ are given in terms of $G_{1,2}^{(u_f)}$.

$$
\begin{aligned}
C_1^{(u_f)\mu} = \int dV_R \frac{R^\mu}{u_f - m_{d'}^2} &= G_1^{(u_f)} \not{p}_T + G_2^{(u_f)} \left(\not{q}' - \frac{s - m_{a'}^2 + \widetilde{m}_{b'}^2}{2s} \not{p}_T\right) = F_1^{(u_f)} \not{p}_T + F_2^{(u_f)} \not{q}' \,, \\
G_1^{(u_f)} = \frac{1}{s} C_{1p_T}^{(u_f)} \,, \quad G_2^{(u_f)} &= -\frac{4s}{\omega(s, m_{a'}^2, \widetilde{m}_{b'}^2)^2} \left(C_{1q'}^{(u_f)} - \frac{s - m_{a'}^2 + \widetilde{m}_{b'}^2}{2s} C_{1p_T}^{(u_f)}\right), \\
F_1^{(u_f)} = G_1^{(u_f)} - \frac{s - m_{a'}^2 + \widetilde{m}_{b'}^2}{2s} G_2^{(u_f)} \,, \quad F_2^{(u_f)} &= G_2^{(u_f)} \,.
\end{aligned}
\tag{6}
$$

For integrals of type $C^{(u_i)}$ (diagrams *uc* and *us* in fig. 1) the integrand depends on $u_i = (R - q)^2$. The kinematic limits $u_{i\substack{\max\\\min}}$ for u_i are obtained from $u_{\substack{\max\\\min}}$ in (30) with the substitutions $a' \to h$, $b' \to h'$. The scalar integrals $C_0^{(u_i)}$, $C_{1p_T}^{(u_i)}$ and $C_{1q}^{(u_i)}$, as well as the vector integral $C_1^{(u_i)\mu}$ and its form factors $G_{1,2}^{(u_i)}$, $F_{1,2}^{(u_i)}$ are obtained from (3)–(6) by means of the substitutions $a' \to a$, $b' \to b$, $d' \to d$, $p' \to p$, $q' \to q$, $u_f \to u_i$, $u_{f\substack{\max\\\min}} \to u_{i\substack{\max\\\min}}$.

B.3 Box diagram

The basic scalar box integral is given by

$$D_0 = \int dV_R \frac{1}{u_f - m_{d'}^2}\frac{1}{u_i - m_d^2} = 4\pi\theta(\sqrt{s} - (m_h + \widetilde{m}_{h'}))\frac{|\vec{R}|_{\rm cm}}{\sqrt{s}\sqrt{\mathcal{D}_{fi}^2 - 4\mathcal{D}_f\mathcal{D}_i}}\text{Argtanh}\left(\sqrt{\frac{\mathcal{D}_{fi} - 2\sqrt{\mathcal{D}_f\mathcal{D}_i}}{\mathcal{D}_{fi} + 2\sqrt{\mathcal{D}_f\mathcal{D}_i}}}\right),$$

$$|\vec{R}|_{\rm cm} = \frac{\omega(s, m_h^2, \widetilde{m}_{h'}^2)}{2\sqrt{s}}\ , \qquad (\vec{q}\,'\cdot\vec{q})_{\rm cm} = \frac{1}{2}\left(\frac{u_{\rm max} + u_{\rm min}}{2} - u\right),$$

$$\mathcal{D}_f = (m_{d'}^2 - u_{f_{\rm max}})(m_{d'}^2 - u_{f_{\rm min}}), \qquad \mathcal{D}_i = (m_d^2 - u_{i_{\rm max}})(m_d^2 - u_{i_{\rm min}}),$$

$$\mathcal{D}_{fi} = \frac{1}{2}(2m_{d'}^2 - u_{f_{\rm max}} - u_{f_{\rm min}})(2m_d^2 - u_{i_{\rm max}} - u_{i_{\rm min}}) - 8|\vec{R}|_{\rm cm}^2\left(\vec{q}\,'\cdot\vec{q}\right)_{\rm cm}\ . \tag{7}$$

For all diagrams allowed by conservation laws we must have $u_{f_{\rm max}} \le m_{d'}^2$, $u_{i_{\rm max}} \le m_d^2$ due to the stability of ground-state baryons against strong decay, therefore $\mathcal{D}_f \ge 0 \le \mathcal{D}_i$. Furthermore, it can be seen from its definition above that within the physical region $\mathcal{D}_{fi} \ge 2\sqrt{\mathcal{D}_f\mathcal{D}_i}$. From (7), by algebraic reduction we get,

$$D_{1p_T} = \int dV_R \frac{R\cdot p_T}{(u_f - m_{d'}^2)(u_i - m_d^2)} = \frac{1}{2}(s + m_h^2 - \widetilde{m}_{h'}^2)D_0\ , \tag{8}$$

$$D_{1q} = \int dV_R \frac{R\cdot q}{(u_f - m_{d'}^2)(u_i - m_d^2)} = \frac{1}{2}(m_h^2 + \widetilde{m}_b^2 - m_d^2)D_0 - \frac{1}{2}C_0^{(u_f)}\ , \tag{9}$$

$$D_{1q'} = \int dV_R \frac{R\cdot q'}{(u_f - m_{d'}^2)(u_i - m_d^2)} = \frac{1}{2}(m_h^2 + \widetilde{m}_{b'}^2 - m_{d'}^2)D_0 - \frac{1}{2}C_0^{(u_i)}\ . \tag{10}$$

As with triangle diagrams, we decompose the vector integral into two sets of form factors, $G_i^{(uu)}$ and $F_i^{(uu)}$,

$$D_1^\mu = \int dV_R \frac{R^\mu}{(u_f - m_{d'}^2)(u_i - m_d^2)} = G_1^{(uu)}\not{p}_T + G_2^{(uu)}\not{v}_2 + G_3^{(uu)}\not{v}_3 = F_1^{(uu)}\not{p}_T + F_2^{(uu)}\not{q} + F_3^{(uu)}\not{q}\,'\ ,$$

$$v_2 = q - \frac{1}{2s}(s + \widetilde{m}_b^2 - m_a^2)p_T\ , \quad v_3 = q' - \frac{1}{2s}(s + \widetilde{m}_{b'}^2 - m_{a'}^2)p_T + \frac{2s}{\omega(s, m_a^2, \widetilde{m}_b^2)^2}\left(u - \frac{u_{\rm max} + u_{\rm min}}{2}\right)v_2\ . \tag{11}$$

Calling $v_1 = p_T$ we have $v_i\cdot v_j \propto \delta_{ij}$, $i, j = 1, 2, 3$. The vectors v_i are obtained from p_T, q, q' by Gramm–Schmidt orthogonalization for simplicity. More symmetrical results can be obtained with the orthogonalization method of [35]. The form factors are given by,

$$\begin{aligned}
G_1^{(uu)} &= \frac{s + m_h^2 - \widetilde{m}_{h'}^2}{2s}D_0\ ,\\
G_2^{(uu)} &= \frac{-4s}{\omega(s, m_a^2, \widetilde{m}_b^2)^2}\left(D_{1q} - \frac{1}{2s}(s + \widetilde{m}_b^2 - m_a^2)D_{1p_T}\right),\\
G_3^{(uu)} &= \frac{\omega(s, m_a^2, \widetilde{m}_b^2)^2}{s(t - t_{\rm max})(t - t_{\rm min})}\left(D_{1q'} - \frac{1}{2}(s + \widetilde{m}_{b'}^2 - m_{a'}^2)G_1^{(uu)} - \frac{1}{2}\left(u - \frac{u_{\rm max} + u_{\rm min}}{2}\right)G_2^{(uu)}\right),\\
F_1^{(uu)} &= G_1^{(uu)} - \frac{s + \widetilde{m}_b^2 - m_a^2}{2s}G_2^{(uu)} - \frac{s + \widetilde{m}_{b'}^2 - m_{a'}^2}{2s}G_3^{(uu)} - \frac{s + \widetilde{m}_b^2 - m_a^2}{\omega(s, m_a^2, \widetilde{m}_b^2)^2}\left(u - \frac{u_{\rm max} + u_{\rm min}}{2}\right)G_3^{(uu)}\ ,\\
F_2^{(uu)} &= G_2^{(uu)} + \frac{2s}{\omega(s, m_a^2, \widetilde{m}_b^2)^2}\left(u - \frac{u_{\rm max} + u_{\rm min}}{2}\right)G_3^{(uu)}\ ,\\
F_3^{(uu)} &= G_3^{(uu)}\ .
\end{aligned} \tag{12}$$

From the definition of D_1^μ in (11) it is clear that under exchange of initial and final state ($a \leftrightarrow a'$, $b \leftrightarrow b'$, $q \leftrightarrow q'$, $p \leftrightarrow p'$, etc.) we must have $F_1^{(uu)} \leftrightarrow F_1^{(uu)}$ and $F_2^{(uu)} \leftrightarrow F_3^{(uu)}$. In the expressions (12) for $F_{1,2,3}^{(uu)}$ this symmetry is not apparent, but it has been checked numerically.

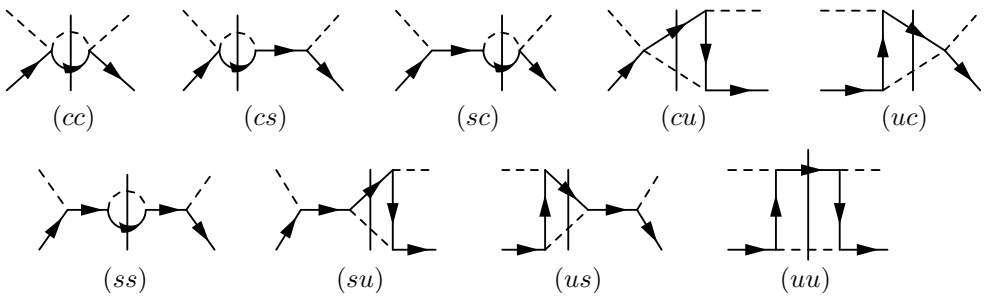

Figure 1: Feynman diagrams contributing to the absorptive part of the scattering amplitude. Vertical lines denote unitary cuts factoring each diagram into two tree-level diagrams as indicated by the labels.

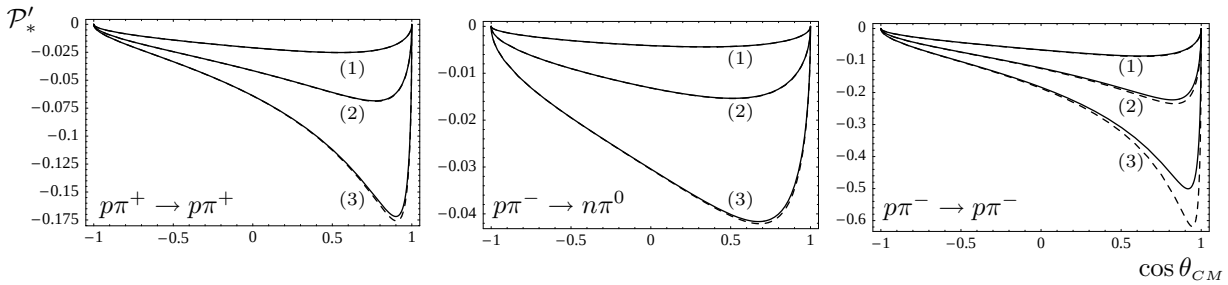

Figure 2: BChPT result for the polarization of the final baryon in its rest frame as a function of center-of-mass scattering angle. Solid lines: $\mathcal{P}'_*$, dashed lines:$\mathcal{P}'_{*\text{l.o.}}$ (see sect. 4). Curves (1)–(3) correspond to lab frame initial meson momentum $q_{\text{lab}} = 75$, 100, 125 MeV, resp.

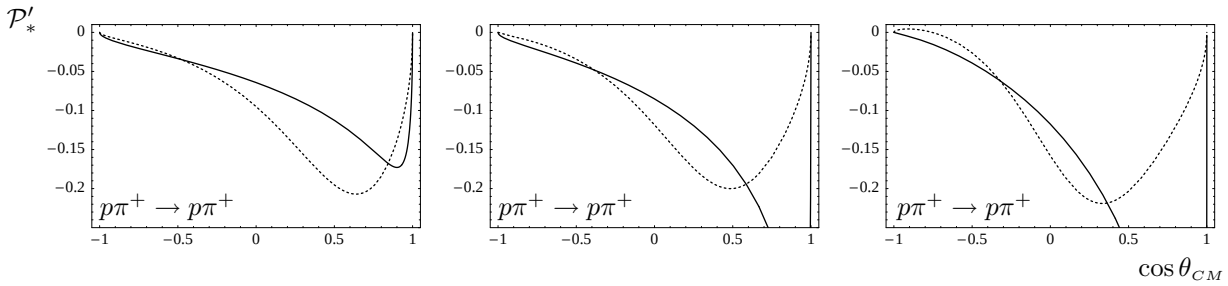

Figure 3: Solid lines as in fig. 2, dotted lines: $\mathcal{P}'_*$ including Δ resonance. From left to right, $q_{\text{lab}} = 125$, 150, 200 MeV.

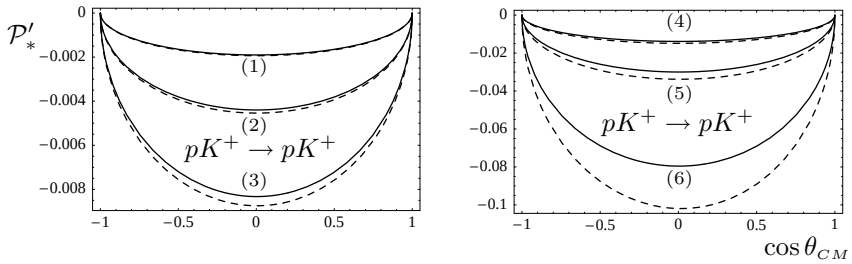

Figure 4: Solid and dashed lines as in fig. 2. Curves (1)–(6): $q_{\text{lab}} = 75$, 100, 125, 150, 200, 300 MeV, resp.

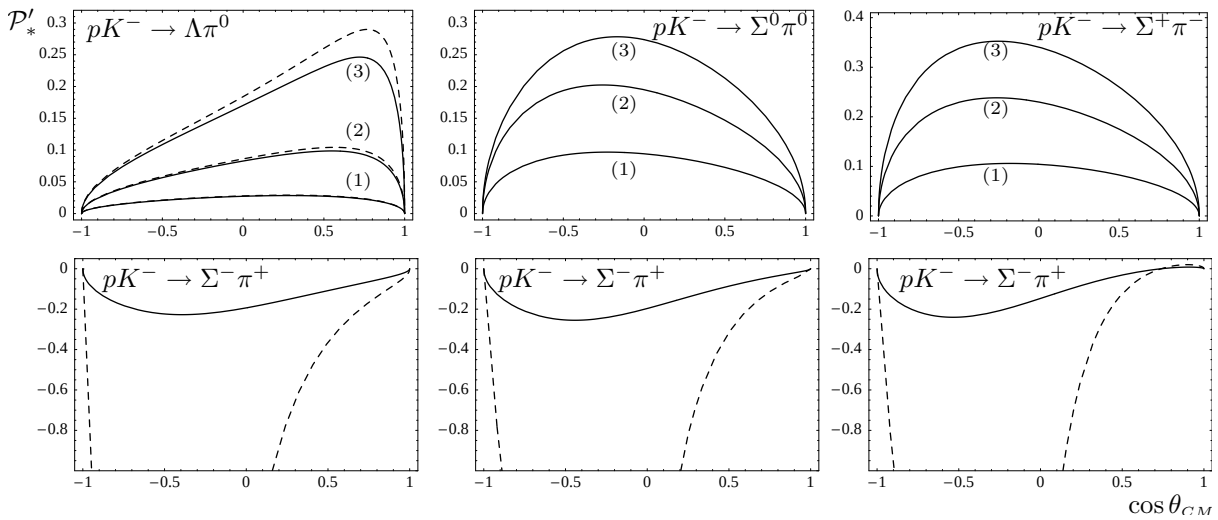

Figure 5: Solid and dashed lines (not shown in some plots for clarity) as in fig. 2. Upper row, curves (1)–(3): $q_{\rm lab} = 100$, 200, 300 MeV, resp. Lower row, from left to right: same values of $q_{\rm lab}$.

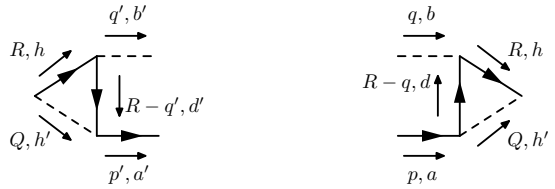

Figure 6: Labelling of momenta and flavors in triangle graphs with final- and initial-state particles attached.